Academic Science Journal

Synthesis and Characterization of $(Ni,Co)_xMn_{0.25-x}Mg_{0.75}Fe_2O_4$ Nanoparticles

Hussein I. Mahdi [1*], Nabeel A. Bakr [1], Tagreed M. Al-Saadi [2]

[1] Department of Physics, College of Science, University of Diyala, Diyala, IRAQ

[2] College of Education for Pure Science, Ibn Al Haitham, University of Bagdad, Bagdad, IRAQ

[*]sciphydr2110@uodiyala.edu.iq

Received: 30 March 2023 **Accepted: 12 May 2023**

DOI: https://doi.org/10.24237/ASJ.02.02.751C

Abstract

Ni-Co-Mn-Mg ferrite nanoparticles with the formula $(Ni,Co)_xMn_{0.25-x}Mg_{0.75}Fe_2O_4$ were synthesized in this work by employing the sol-gel auto-combustion process, with nitrates used as the cations source and citric acid ($C_6H_8O_7$) as the combustion agent. X-ray diffraction (XRD), field emission scanning electron microscopy (FE-SEM), energy dispersive X-ray (EDX), and a vibrating sample magnetometer (VSM) were used to characterize the structural, morphological, and magnetic properties of ferrite powders. The XRD measurements showed crystallite sizes ranging between 24 - 28 nm. The FE-SEM images show the presence of agglomeration as well as a non-homogeneous distribution of the samples. On the other hand, the stoichiometry of the reactant solutions that were used is in close agreement with the elemental analysis that was obtained from EDX showing that the composition was as expected. Manganese ferrite showed a decrease in magnetic parameters on magnesium doping, which was further enhanced in $(Ni,Co)_xMn_{0.25-x}Mg_{0.75}Fe_2O_4$ nanoparticles upon replacement of nonmagnetic manganese ions for nickel and cobalt ions. Results indicated that Ni-Co-Mn-Mg ferrite nanoparticles' crystal morphology, structural, and magnetic properties were significantly influenced by the amounts of nickel and cobalt content.

Keyword: Mn-Mg Ferrite, Sol-gel process, Structure characterization, Magnetic measurements.

Academic Science Journal

تحضير وتوصيف المركب الفرايتي $(Ni,Co)_xMn_{0.25-x}Mg_{0.75}Fe_2O_4$ النانوي

حسين اسماعيل مهدي[1], نبيل علي بكر[1], تغريد مسلم مريوش[2]

[1] قسم الفيزياء — كلية العلوم — جامعة ديالى

[2] قسم الفيزياء — كلية التربية ابن الهيثم — جامعة بغداد

الخلاصة

في هذا العمل تم تصنيع مركب الفرايت Ni-Co-Mn-Mg النانوي ذي الصيغة $(Ni,Co)_xMn_{0.25-x}Mg_{0.75}Fe_2O_4$ من خلال استخدام تقنية الاحتراق التلقائي (sol-gel) ، حيث تعمل النترات كمصدر للكاتيونات وحامض الستريك $(C_6H_8O_7)$ كعامل احتراق. تم استخدام طيف حيود الأشعة السينية (XRD) ، والمطياف الالكتروني الماسح لانبعاث المجال (FE-SEM) ، وحيود الأشعة السينية المشتتة للطاقة (EDX) ، ومقياس نموذج الاهتزاز المغناطيسي (VSM) لتوصيف الخصائص التركيبية والمورفولوجية والمغناطيسية لمساحيق الفرايت. أظهرت قياسات XRD أحجاما بلورية تتراوح بين 24 - 28 نانومتر. تُظهر صور FE-SEM وجود تكتل بالإضافة إلى توزيع غير متجانس للعينات. من ناحية أخرى، فإن القياس المتكافئ لمحاليل المتفاعل التي تم استخدامها في اتفاق وثيق مع التحليل الأولي الذي تم الحصول عليه من EDX والذي يوضح أن التركيبة كانت كما هو متوقع. أظهر فرايت المنغنيز المشوب بالمغنيسيوم انخفاضًا في المعلمات المغناطيسية، والتي تم تحسينها بشكل أكبر في $(Ni,Co)_xMn_{0.25-x}Mg_{0.75}Fe_2O_4$ عند استبدال أيونات المنغنيز غير المغناطيسية لأيونات النيكل والكوبالت. أشارت النتائج إلى أن الخصائص المجهرية لمركب Ni-Co-Mn-Mg ferrite النانوي، والخصائص التركيبية والمغناطيسية، تأثرت بشكل كبير بكميات محتوى النيكل والكوبالت.

كلمات مفتاحية: Mn-Mg Ferrite, تقنية الاحتراق التلقائي (sol-gel), الخصائص التركيبة, قياسات المغناطيسية.

Introduction

Several significant areas of technology, including ferrofluids, magnetic medicine delivery, and high-density information storage, are showing an increased interest in magnetic nanoparticles [1]. Recently, they have also been used as contrast agents for magnetic resonance imaging (MRI) in biomedical fields, high-speed integrated circuits, and nano-electronic devices [2–5]. Given the wide variety of possible applications, from fundamental research to industrial applications, nanoscale magnetic oxides have recently attracted a lot of interest.

Nanoparticles of spinel ferrite are particularly important among these materials. Fe_3O_4 (also known as spinel ferrite) is one of the superparamagnetic metal oxides with the general formula MFe_2O_4 (M=Co, Mn, Zn, Ni, Mg, etc.), oxygen is packed in a face-centered cubic (FCC) lattice, and M^{2+} and Fe^{3+} ions can occupy either octahedral (B) and also tetrahedral (A) interstitial sites, respectively [6,7]. They exhibit a range of magnetic characteristics depending on the composition and cation distribution. Different cations can be placed into their A and B sites to change their magnetic characteristics. Magnesium ferrite ($MgFe_2O_4$) nanoparticles are a potential candidate among spinel ferrites for various applications, including absorbing materials, photo-catalysts, gas sensors, and materials that absorb electromagnetic waves [8,9]. However, various factors can affect the magnetic characteristics of nanoparticles, including the preparation process, grain size, form, and composition. Thus, the capacity to control the form and size of nanomaterials is fundamental to governing their magnetic characteristics and meeting scientific and innovative needs [10]. As a result of its advantages, the sol-gel technology is one of the most efficient and successful techniques to fabricate nanoscale ferrite materials including high stoichiometric control and the ability to produce nano-particles with a tight size distribution in a small amount of time at a very low temp [4,11].

This study reports on research into the influences of nickel and cobalt substitution on the structural, morphological, and magnetic characteristics of manganese-magnesium ferrite synthesized via (sol-gel) auto-combustion technique.

Experimental

1. Preparation of Ni-Co-Mn-Mg-Fe_2O_4 nanoparticles powders

Ni-Co-Mn-Mg ferrites with the chemical formula $(Ni,Co)_xMn_{0.25-x}Mg_{0.75}Fe_2O_4$ (x = 0.00, 0.10, and 0.20) were synthesized by using the sol-gel auto combustion method. The desirable proportions of the initial ingredients were used for the combustion reaction, which included citric acid $C_6H_8O_7$ (M_w=192.13), manganese nitrate $Mn(NO_3)_2.H_2O$ (M_w=189.00), magnesium nitrate $Mg(NO_3)_2.6H_2O$ (M_w=256.41), ferric nitrate $Fe(NO_3)_3.9H_2O$ (M_w=404.00), and highly

pure (99%) Analytical-grade (India). Table 1 shows the required masses of the raw materials needed to prepare the ferrite. The following equation is used to obtain these values:

$$Wt = M_w \times M \times W \quad \ldots\ldots\ldots\ldots\ldots\ldots (1)$$

Where W_t is the raw material's mass (g), M_w is the raw material's molecular weight (g/mol), M is the number of moles (mol/L), and W is the solvent volume (L).

A magnetic stirrer was used to dissolve all reagents in deionized water to form a mixed solution, which was then agitated for 30 min to improve homogeneity and produce what is known as a precursor. Citric acid was added in a 1:1 molar ratio to the metal ions present in the composition to convert the nitrate mixed solution into citrate solution. Diluted NH_3 solution was added drop by drop to the resulting solutions until had a pH of ~7 to promote the reactants faster quickly and actively. At one point, the material undergoes auto-ignition and combustion, thereby becoming a fluffy ferrite mass; from there, it is transformed into nano-sized particles via the emission of reddish-brown gases at temperatures of around 180 °C. Finally, the powder was sintered for 2 hours at 600 °C.

Table 1: The masses of raw materials required to obtain $(Ni,Co)_xMn_{0.25-x}Mg_{0.75}Fe_2O_4$ nanoparticles.

X	FERRIC NITRATE (G)	MAGNESIUM NITRATE (G)	MANGANESE NITRATE (G)	NICKEL NITRATE (G)	COBALT NITRATE (G)	CITRIC ACID (G)
0.00	32.32	7.6923	1.8900	0.00	0.00	23.0556
0.10	32.32	7.6923	1.1340	0.5816	0.5820	23.0556
0.20	32.32	7.6923	0.3780	1.1632	1.1641	23.0556

2. Characterization of Ni-Co-Mn-Mg-Fe_2O_4

Using an X-ray diffractometer (model: Philips PW1730) and Cu-Kα (λ= 1.5406 Å) radiation recorded in the range of 20º–80º, the crystal structure of the samples was characterized. The ferrite samples' surface morphology was analyzed using field emission scanning electron microscopy (FE-SEM, MTRA3 LMU). Energy-dispersive X-ray spectroscopy was used to

determine the composition (EDX, OXFORD INSTRUMENTS). Analysis of magnetic properties was conducted at room temperature using a vibrating sample magnetometer (EZ VSM model 10), with a maximum applied magnetic field of 10 KOe.

Results and Discussion

1. Structural characteristics

The Debye-Scherrer equation is used to calculate the crystallite size from the FWHM for the most intense (311) peak in the XRD pattern [12,13]:

$$D = 0.9\lambda/\beta\cos\theta \quad \text{…….. (2)}$$

Where θ is the Bragg's angle and λ is the wavelength of the XRD, meanwhile, β is the FWHM of the strongest intensity (311) peak.

Using the following relationship, the lattice constant (a) was determined [14,15]:

$$a = d_{hkl}\sqrt{h^2 + k^2 + I^2} \quad \text{…….. (3)}$$

Where *hkl* represented the miller indices and d represented the inter-planer distance.

The following relation was used to determine the x-ray density ρ_x [16]:

$$\rho_x = \frac{z\,M_w}{N_A\,a^3} \quad \text{…… (4)}$$

Where Z for the spinel system is the number of molecules in a unit of formula (Z = 8), M_w is the molecular weight of the sample, and N_A is the Avogadro's number ($N_A = 6.023 \times 10^{23}$) atom/mole, while a^3 is the cubic structure's volume per cubic unit cell.

Figure 1 shows the XRD patterns of the $(Ni,Co)_xMn_{0.25-x}Mg_{0.75}Fe_2O_4$ nanoparticles as synthesized. Herein, with the corresponding diffraction peaks of (220), (311), (400), (422), (511), (440), and (533) crystal planes, prominent Bragg reflections in this instance can be indexed as face-centered cubic (FCC) spinel type structure, and they are in good agreement with JCPDS card 89–3084 [17]. In all the samples, no other impurity phases were detected. In

other words, all of the Ni-Co-Mn-Mg ferrite nanoparticles that were formed had the *Fd-3m* space group and were all of the spinel phases. Meanwhile, the sharp and strong XRD reflections demonstrate the excellent crystallization of the samples. In addition, the lattice parameter and crystallite size of the samples can be estimated using the XRD data [18]. Furthermore, the crystallite size gradually decreased as Ni and Co doping increased. The XRD pattern revealed this, the peaks shifting to the right side as the θ value was increased caused by Ni and Co substitution [19], as listed in Table 2. Table 3 shows the crystallite size (D), lattice constant (a), and density (ρ_x) for all samples. As shown, when Ni^{+2} and Co^{2+} content in Mn-Mg ferrites increases, hence, increases the lattice constant. Due the atomic radius varies from one metal to another, the lattice constant increased as the concentration of Mn decreased, such as nickel (0.69 Å), cobalt (0.67 Å), and manganese (0.83 Å). Consequently, causing the elongation or compression of the crystal lattice [20,21].

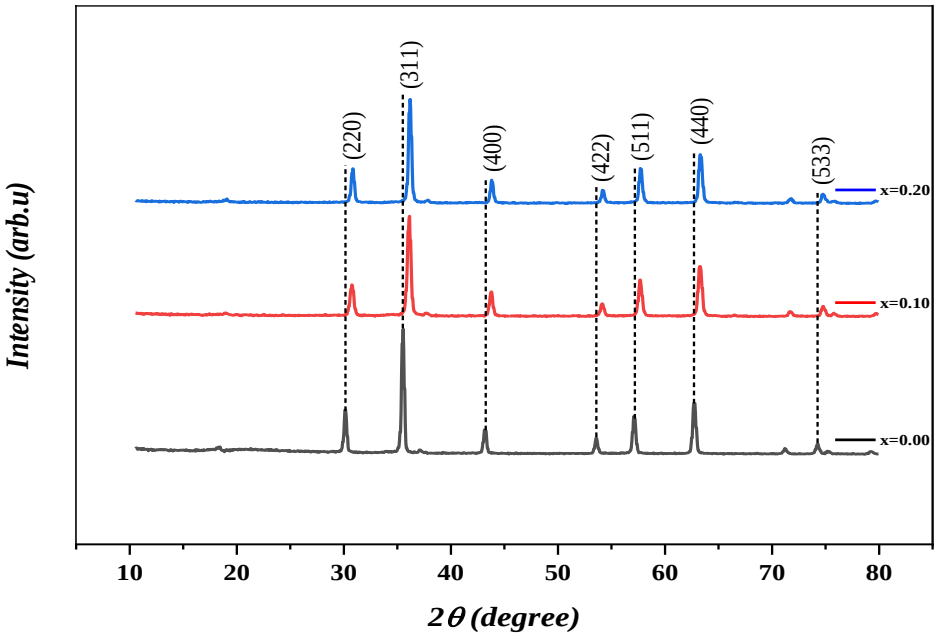

Figure 1: XRD patterns of $(Ni,Co)_xMn_{0.25-x}Mg_{0.75}Fe_2O_4$ nanoparticles

Table 2: Structure properties of the $(Ni,Co)_xMn_{0.25-x}Mg_{0.75}Fe_2O_4$ nanoparticles

H K L	2Θ (DEG) (X=0.00)	2Θ (DEG) (X=0.10)	2Θ (DEG) (X=0.20)
220	30.1365	30.4393	30.3890
311	35.4950	35.6485	35.7397
400	43.2299	43.3704	43.4431
422	53.5835	53.7058	53.8056
511	57.1528	57.2586	57.3520
440	62.7239	62.8588	62.9471
533	74.2529	74.3487	74.2970

Table 3: XRD parameters of the $(Ni,Co)_xMn_{0.25-x}Mg_{0.75}Fe_2O_4$ nanoparticles

X	COMPOSITION	A (Å)	P (G/CM^3)	D (NM)
0.00	$Mn_{0.25}Mg_{0.75}Fe_2O_4$	8.3674	5.250	28.31
0.10	$(Ni,Co)_{0.10}Mn_{0.15}Mg_{0.75}Fe_2O_4$	8.3799	5.227	24.30
0.20	$(Ni,Co)_{0.20}Mn_{0.05}Mg_{0.75}Fe_2O_4$	8.3906	5.207	24.30

2. Morphological characteristics and EDX studies

Figure 2 shows the surface morphology of $(Ni,Co)_xMn_{0.25-x}Mg_{0.75}Fe_2O_4$ nanoparticles as studied by FE-SEM at a scale of 10 µm after annealing at 600 °C. Based on the figure, a nonhomogeneous distribution of the particle size with some agglomeration can be attributed to the fact that the particles were exposed to a permanent magnetic moment that was proportionate to their size [22,23]. During the combustion process, a significant quantity of toxic gas is emitted like oxygen و nitrogen, and carbon dioxide, which causes the powders to developing pores, voids, and fractured surfaces, and is often absent from most other synthetic techniques products [24,25]. These features are visible in scanning electron microscopy of the prepared powders.

Academic Science Journal

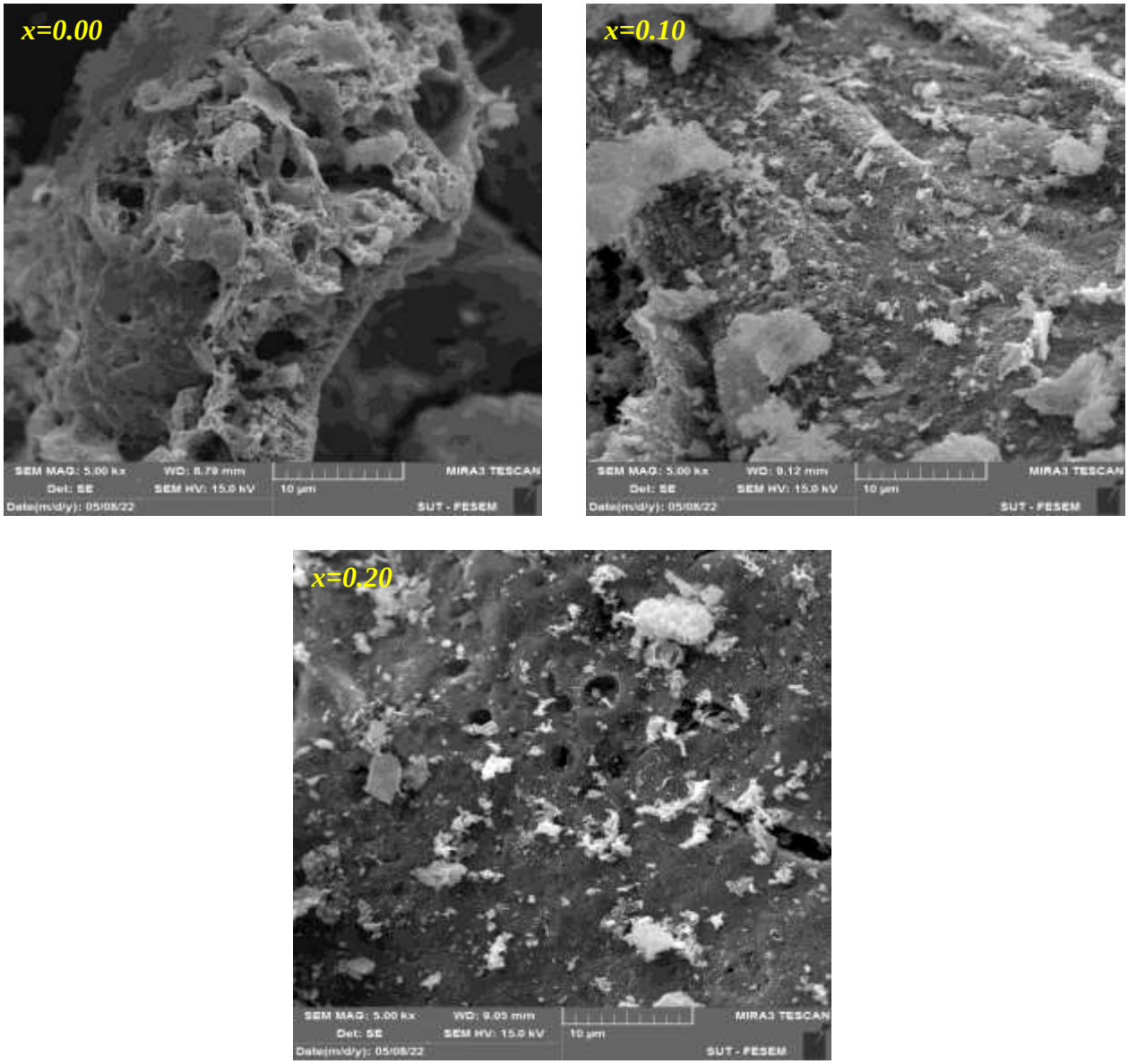

Figure 2: FE-SEM images of $(Ni,Co)_xMn_{0.25-x}Mg_{0.75}Fe_2O_4$ nanoparticles

EDX was used to determine the chemical composition of the sample to confirm our observations about the structure of the $(Ni,Co)_xMn_{0.25-x}Mg_{0.75}Fe_2O_4$ nanoparticles. Figure 3, shows the results of the EDX analysis of typical samples (x = 0.00, 0.10, and 0.20). As shown, the x = 0.00 sample shows no trace of Ni^{2+} and Co^{2+} ions, however, the concentration of Mn^{+2} is very high. On the contrary, the maximum composition of Ni^{2+} and Co^{2+} ions can be observed

for the sample (x = 0.20). Table 4 illustrates the energy Dispersive X-ray analysis of $(Ni,Co)_xMn_{0.25-x}Mg_{0.75}Fe_2O_4$ nanoparticles the sintered at 600 °C. The investigated samples' atomic weight percentages of different cations are approximately correct and correspond to the ratios anticipated by the preparation technique.

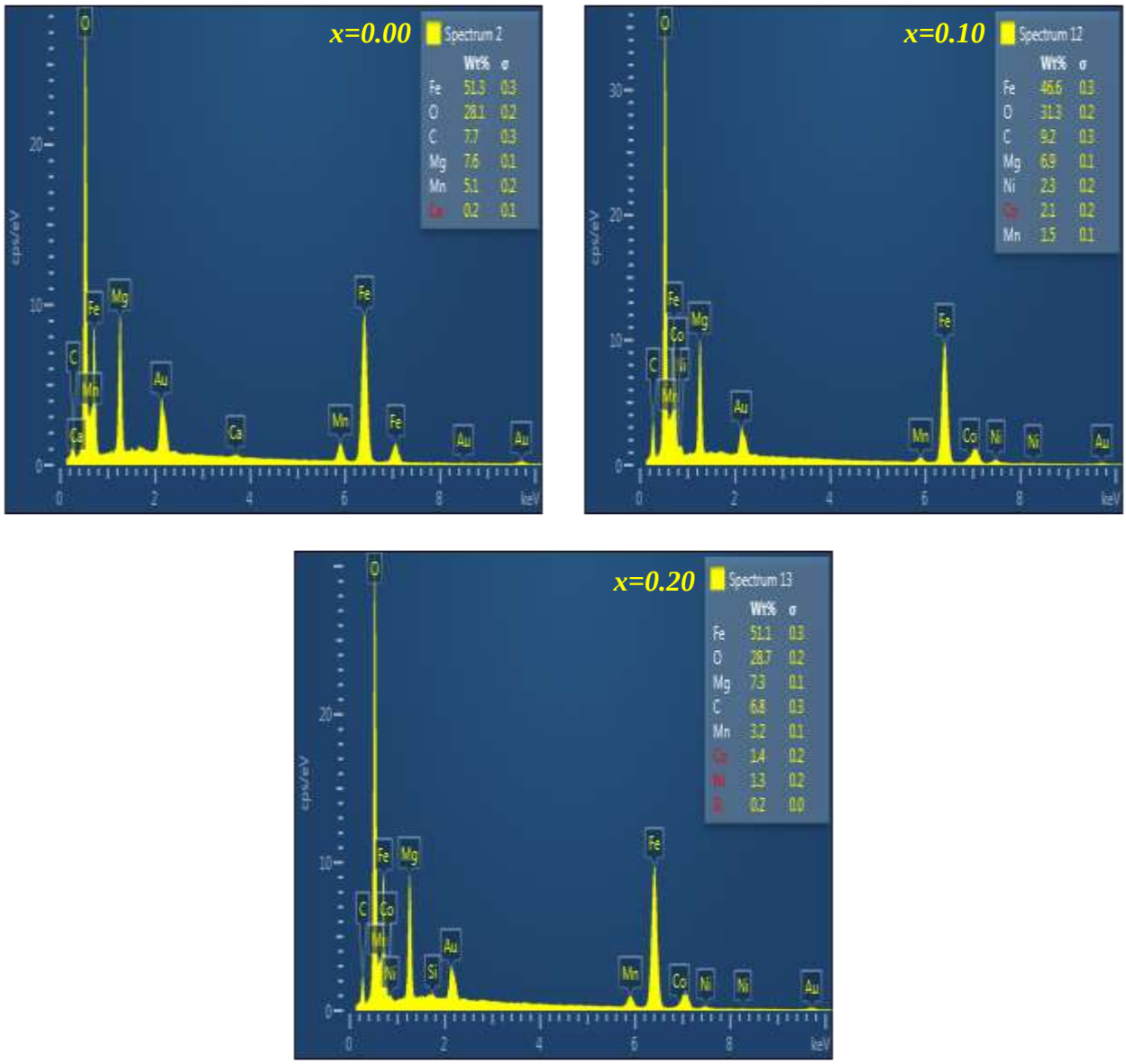

Figure 3: EDX patterns of $(Ni,Co)_xMn_{0.25-x}Mg_{0.75}Fe_2O_4$ nanoparticles

Academic Science Journal

Table 4: Energy Dispersive X-ray analysis of $(Ni,Co)_xMn_{0.25-x}Mg_{0.75}Fe_2O_4$ nanoparticles

$MN_{0.25}MG_{0.75}FE_2O_4$			$(NI,CO)_{10}MN_{0.15}MG_{0.75}FE_2O_4$			$(NI,CO)_{0.20}MN_{0.05}MG_{0.75}FE_2O_4$		
Element	Wt (%)	At (%)	Element	Wt (%)	At (%)	Element	Wt (%)	At (%)
O	28.13	47.15	O	31.29	49.56	O	28.67	48.62
Mg	7.56	8.33	Mg	6.94	7.23	Mg	7.29	8.13
Mn	5.06	2.47	Mn	1.47	0.68	Mn	3.24	1.60
Fe	51.31	24.64	Fe	46.64	21.16	Fe	51.12	24.83
C	7.73	17.27	Co	2.11	0.91	Co	1.36	0.63
Ca	0.21	0.14	Ni	2.33	1.00	Ni	1.32	0.61
			C	9.22	19.46	C	7.00	15.60
Total	100.00	100.00	Total	100.00	100.00	Total	100.00	100.00

3. Magnetic studies

Table 5 shows the effect of varying the stoichiometry on the magnetic parameters of $(Ni,Co)_xMn_{0.25-x}Mg_{0.75}Fe_2O_4$ (x = 0.00 and x = 0.20) as measured by VSM. For the prepared ferrite samples, hysteresis plots were drawn to display the variation in magnetization (M, emu/g) as a function of the magnetic field (H, O_e) (Figure 4). Narrow hysteresis loops were observed (S-shaped) in all of the samples. The samples' magnetic properties, such as saturation magnetization, remnant magnetization, and coercivity, which depend on several factors such as density, anisotropy, particle size, and A-B exchange interactions were also compared. The narrow loop showed low coercivity values between 61.50 O_e and 81.76 O_e.

M_s, M_r, and H_c values of pure manganese magnesium ferrite were 29.00 emu/g, 10.95 emu/g, and 61.50 Oe, respectively. Doping Mn-Mg ferrite with Co^{2+} and Ni^{2+} causes a monotonic increase in saturation magnetization, remnant magnetization, and coercivity, and this is consistent with the findings of researchers [26,27]. The increase in saturation magnetization at this stage can be explained by Neel's theory of ferrimagnetism [28]. Saturation magnetization, which occurs at low concentrations of non-magnetic ions, is described by the formula [29,30]:

$$M_S = \left| M_B - M_A \right| \quad \text{..... (5)}$$

Sites B and A ion magnetization are indicated by M_B and M_A, respectively. The non-magnetic properties of the Ni^{2+} and Co^{2+} ions are responsible for the increase in saturation magnetization

that occurs during doping [29]. Saturation magnetization is increased when non-magnetic nickel and cobalt ions are present in tetrahedral sites and because of polarization effects. The preference of Ni^{2+} and Co^{2+} ions for A sites also facilitates the ability for Fe^{3+} ions to move into B sites, which results in the antiparallel spin coupling, which weakens A–B exchange interactions and increases the saturation magnetization value.

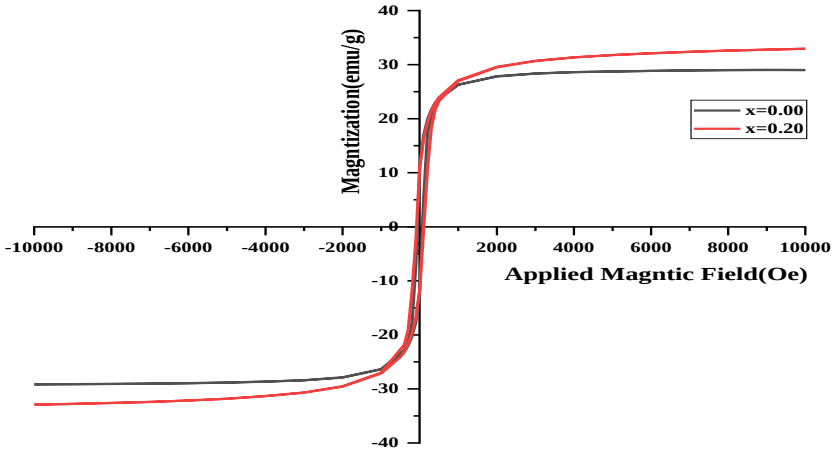

Figure 4: Magnetic hysteresis loops of $(Ni,Co)_xMn_{0.25-x}Mg_{0.75}Fe_2O_4$ nanoparticles

Table 5: Magnetic parameters of $(Ni,Co)_xMn_{0.25-x}Mg_{0.75}Fe_2O_4$ nanoparticles

X	SAMPLE	M_S(EMU/G)	M_R(EUM/G)	$H_C(O_E)$	SQR=MR/MS
0.00	$Mn_{0.25}Mg_{0.75}Fe_2O_4$	29.00	10.95	61.50	0.37
0.20	$(Ni,Co)_{0.20}Mn_{0.05}Mg_{0.75}Fe_2O_4$	32.94	11.24	81.76	0.34

Conclusion

Using the sol-gel auto combustion method, high-performance $(Ni,Co)_xMn_{0.25-x}Mg_{0.75}Fe_2O_4$ nanoparticles have been successfully prepared. Ni-Co Mn Mg ferrite nanoparticles formed a single-phase cubic spinel structure using XRD. FE-SEM findings show nonhomogeneous grain distribution and good connection of the grain. The energy-dispersive X-ray elemental analysis

is in close agreement with the composition expected by the stoichiometry of the reactant solutions utilized. Manganese ferrite showed a decrease in the magnetic parameters on magnesium doping, which was further improved in $(Ni,Co)_xMn_{0.25-x}Mg_{0.75}Fe_2O_4$ nanoparticles on replacement of nonmagnetic manganese ions for nickel and cobalt ions. Nanoparticles of $(Ni,Co)_xMn_{0.25-x}Mg_{0.75}Fe_2O_4$ with a high Ms value indicated that they may be used to produce ferrofluid. The combustion process provides a low-temperature, facile route for the synthesis and structural analysis of Ni-Co-Mn-Mg ferrite nanoparticles.

References

1. Y. Köseoglu, A. Baykal, F. Gözüak, H. Kavas, Polyhedron., 28(14), 2887-2892(2009)
2. W. Yan, Q. Li, H. Zhong, Z. Zhong, Powder Technol., 192(1), 23–26(2009)
3. M. Javed Iqbal, Z. Ahmad, T. Meydan, Y. Melikhov, J. Appl. Phys., 111(3), 033906(2012)
4. M. Srivastava, S. Chaubey, A. K. Ojha, Mater. Chem. Phys., 118(1), 174–180(2009)
5. A. Rafferty, Y. Gun'ko, R. Raghavendra, Mater. Res. Bull., 44(4), 747–752(2009)
6. S. M. Hussein, T. H. Mubarak, S. M. Ali Ridha, J. Al-Zanganawee, Key. Eng. Mater., 882, 200-218(2021)
7. A. Baykal, N. Kasapog˘lu, Y. Köseog˘lu, A. Basaran, H. Kavas, M. Toprak, Cent. Eur. J. Chem., 6(1), 125-130(2008)
8. P. Hu, D. Pan, X. Wang, J. Tian, J. Wang., S. Zhang, A. A. Volinsky, J. Magn. Magn. Mater., 323(5), 569–573(2011)
9. Y. Xu, Y. Liang, L. Jiang, H. Wu, H. Zhao, D. Xue, J. Nanomater., 2011, 1–5(2011)
10. M. Penchal Reddy, X. B. Zhou, Q. Huang, R. Ramakrishna Reddy, Int J Nano Stud Technol., 3(8), 1-6(2014)
11. M. Niederberger, Acc. Chem. Res., 40(9), 793–800(2007)
12. L. Saheb, T. M. Al-Saadi, J Phys Conf Ser, 2114, 012040, (2021)
13. A. H. Mohammad, C. Mariem, O. Israa, B. Fawzi, I. A. Ahmad, Appl. Phys. A, 126(489), 1-9, 2020

14. M. Lakshmi, K. Vijaya Kumar, K. Thyagarajan, J NANOSTRUCTURE CHEM, 5(4), 365-373(2015)

15. T. M. Al-Saadi, A. K. J. Mustafa, Iraqi J. Sci., 57(1), 145-153, 2016

16. H. S. Mahmood, T. H. Mubarak, S. M. Ali Ridha, J. Al-Zanganawee, AIP Conf Proc,2386, 070006(2022)

17. F. Naaz, H. K. Dubey, C. Kumari, P. Lahiri, SN Appl. Sci., 2(808) (2020)

18. Y. Zhang, Y. Liu, Z. Yang, R. Xiong, J. Shi, J Nanopart Res, 13, 4557–4563(2011)

19. M. Hashim, S. S. Meena, R. K. Kotnala, S. E. Shirsath, P. Bhatt, S. Kumar *et al*, J. Magn. Magn. Mater., 360, 21-33(2014)

20. A. Lassoued, M. B. Hassine, F. Karolak, B. Dkhiil, S. Ammar, A. Gadri, J. Mater. Sci. Mater. Electron., 28(24), 18857-18864(2017)

21. S. Singhal, J. Singh, S. K. Barthwal, K. Chandra, J Solid State Chem, 178(10), 3183–3189(2005)

22. O. A. Ahmed, A. H. Abed, T. M. Al-Saadi, Macromol Symp, 401(1), 2100311(2022)

23. H. El Moussaoui, T. Mahfoud, S. Habouti, K. El Maalam, M. Ben Ali, M. Hamedoun, *et al*, J. Magn. Magn. Mater., 405, 181–186(2016)

24. H. B. Desai, A. Kumar, A. R. Tanna, Eur Chem Bull, 10(3), 186-190(2021)

25. J. Y. Patil, D. Y. Nadargi, I. S. Mulla, S. S. Suryavanshi, Heliyon, 5(6), e01489, 2019

26. R. Chen, W. Wang, X. Zhao, Y. Zhang, S. Wu, F. Li, Chem. Eng. J., 242, 226-233(2014)

27. M. K. Syed, S. Abdul Khader, C. S. Qadeeruddin, Int. J. Mech. Eng. Technol., 7(6), 119-129(2022)

28. M. H. Khedr, A. A. Omar, M. I. Nasr, E. K. Sedeek, J Anal Appl Pyrolysis, 76(1-2), 203-208(2006)

29. M. Kaur, P. Jain, M. Singh, Mater. Chem. Phys., 162, 332-339(2015)

30. O. A. Ahmed, A. H. Abed, T. M. Al-Saadi, Int. Conf. Eng. Sci. Appl. Eng. Mater, 401(1), 2100311, 2022